Nuclear Physics A388 (1982) 452–476

THE BREAKING OF INTRINSIC REFLECTION SYMMETRY IN NUCLEAR GROUND STATES

G.A. LEANDER* and R.K. SHELINE

Florida State University, Tallahassee, Florida

P. MÖLLER, P. OLANDERS and I. RAGNARSSON

Lund Institute of Technology, Lund, Sweden

and

A.J. SIERK

Los Alamos National Laboratory, Los Alamos, New Mexico

Received 13 April 1982

Abstract: Negative-parity excited states of doubly even nuclei have earlier been attributed to vibrational excitations. This paper shows that an interpretation starting from a reflection asymmetric intrinsic state is more appropriate for certain nuclei in the radium region. Theoretical evidence for stable octupole deformation comes from a deformed shell-model calculation in which we use a single-particle potential with a realistic radial shape and a finite-range interaction for the surface energy. The octupole effect systematically improves the agreement between theoretical and experimental masses. The low-lying 0^+ excitations observed in experiment are compatible with the calculated collective octupole potentials. The possibility of obtaining further evidence from the spectroscopy of odd-mass nuclei is considered in an exactly solvable model, which shows that the smaller energy splitting observed in odd-A parity doublets mainly reflects single-particle fragmentation of the collective mode. The systematics of theoretical shell structure and experimental spectroscopy suggests the presence of other regions of octupole collectivity near the limits of stability.

1. Introduction

When very low-lying negative-parity states were discovered in the radium region by Stephens, Asaro and Perlman [1]), the possibility of an octupole surface mode was considered by the Copenhagen group [2]). A continued interest in this topic is motivated by the fact that any nuclear structure theory incorporating the universally dominant quadrupole mode may be differently tested in the octupole case, where the symmetries are different.

The spectroscopy in the radium region indicates [1,2]) that the low-lying octupole mode has $K = 0$, which simplifies calculations in a deformed representation considerably. Using in most cases the Nilsson model with terms $r^2 Y_{20}$ and $r^2 Y_{30}$, numerous calculations have been made to determine the stability of the ground

* Work completed at the present address: UNISOR, Oak Ridge Associated Universities, Oak Ridge, Tennessee, with partial support from DOE under contract DE-Ac05-760R 00033.

state with respect to octupole deformation both in the radium region and other regions of nuclei [3–16]). The unanimous conclusion has been that even–even nuclei with low-lying negative-parity states are indeed soft or slightly unstable with respect to octupole intrinsic deformation, but the intrinsic left–right asymmetry is never well stabilized in the ground state. Consequently many vibrational descriptions have been developed. Models based on purely collective vibrations have not been able to connect with experiment in a satisfactory way [17]), though the boson approach [18–21]) remains to be explored. The random phase approximation has given the best description so far of the octupole states [22–26]).

A recent potential-energy calculation by Möller and Nix [27]), using the folded Yukawa single-particle potential rather than the oscillator, does however exhibit a substantial octupole instability around ^{222}Ra, for the first time in any theoretical calculation. The spectroscopic evidence from the doubly even radium nuclei can also be interpreted to indicate stable octupole deformation. If the very low-lying 1^- level were a member of a $K = 0^-$ vibrational band there would be an $I^\pi = 0^+$ two-phonon vibration at less than twice the energy of the 1^- level. Decay studies [28]) and Coulomb excitation [29]) have failed to reveal any 0^+ states at such low energy.

It may be mentioned that Chasman [30]) has performed diagonalizations based on Woods–Saxon single-particle levels, which may also have resulted in octupole asymmetric states. Due to the use of a reflection symmetric basis, however, there are no obvious criteria for recognizing ground-state asymmetry other than those already applied to the experimental data. Chasman's calculations do reproduce the data quite well in both even and odd nuclei. One very interesting conclusion which he can extract from the wave functions is that the pairing mode plays a significant role for the excited 0^+ levels actually observed in the Ra nuclei.

It may furthermore be mentioned that octupole deformation has recently been obtained in potential-energy calculations by Gyurkovich *et al.* [31]), which are discussed below.

The purpose of the present paper is to demonstrate positive evidence supporting the description of the octupole instability in the folded Yukawa model, and at the same time to establish a framework for future spectroscopic investigations. Potential-energy functions for nuclei in the radium region have been calculated systematically and are described in sect. 2. The systematic effect of the octupole deformation energy on the comparison between theoretical and experimental masses is presented in sect. 3. The potentials are related to $K = 0$ band head energies in sect. 4 and to the parity splitting of the band heads in odd-A nuclei in sect. 5. Other mass regions are discussed in sect. 6.

2. Potential energies

2.1. THE METHOD

The potential energy has been calculated as a function of quadrupole (ε_2), octupole (ε_3) and hexadecapole (ε_4) deformation for nuclei with $84 \leq Z \leq 92$ and

$130 \leq N \leq 148$ using the well-known microscopic–macroscopic method. The single-particle level scheme in a deformed potential is calculated and used to extract the Strutinsky shell correction energy, the BCS pairing energy and for odd or odd–odd nuclei the quasiparticle energy. These terms are added to a macroscopic energy. The procedure is repeated over a lattice in deformation space to define the potential-energy function.

Both the single-particle potential and the macroscopic energy formula in the present work show essential differences from the ones used previously to investigate ground-state octupole deformations. The single-particle potential is of the folded Yukawa type proposed by the Los Alamos group [33]), with parameters fitted by Möller, Nilsson and Nix [27,34]) to a broad data base of empirical quasiparticle energies. The folded Yukawa potential is fairly constant in the interior region, like a Woods–Saxon potential but unlike the modified oscillator used in previous investigations of octupole shapes.

With this in mind it is instructive to consider the general condition for shell closure described by Bohr and Mottelson [35]). Any shell closure in a spherical potential is characterized by an integer ratio $a:b$ corresponding classically to the ratio between the number of radial and angular oscillations in a closed orbit. A 2:1 ratio implies orbits of ellipsoidal type with $\Delta l = 2, 4, 6, \ldots$ between different states in the same shell. Nuclei with large quadrupole moments, hexadecapole moments, etc. are thus naturally formed. A 3:1 ratio implies orbits of triangular type with $\Delta l = 3, 6, \ldots$ in a shell. This favours deformation of octupole type.

The harmonic oscillator has only ellipsoidal closed orbits and 2:1 shell structure while a more flat-bottomed potential may have triangular closed orbits and 3:1 shells for sufficiently large particle numbers. Thus, the octupole shell structure which may be present in a realistic nuclear potential is not present in a harmonic oscillator. In the modified oscillator potential, a l^2 term is introduced to get the same level order as in a flat-bottomed potential. Then there could be more or less the same shell effects as in a flat-bottomed potential.

In the present calculation, using a folded-Yukawa potential, the energy at the octupole deformed minima is found to be 1–2 MeV lower than the energy in the modified oscillator at the same deformation. To further investigate this, we have studied especially the interactions between the suborbitals of the spherical $f_{7/2}$ and $i_{13/2}$ proton shells. In a spherical folded-Yukawa potential these shells come very close to each other, so the interaction due to ε_3 deformation can be extracted numerically, while in the modified oscillator the matrix elements of $r^2 Y_{30}$ are easily calculated analytically. It turns out that the interaction is weaker in the modified oscillator by a factor of about 0.6. Thus, it seems that a deformation ε_3 of the folded-Yukawa potential gives rise to stronger interaction matrix elements than the same deformation ε_3 in the oscillator potential. One way to correct for this in the modified oscillator model would be to renormalize the ε_3 value in relating to a macroscopic shape and the liquid-drop model. This is effectively what is done in the approach of Gyurkovich *et al.* [31]), mentioned above, where the modified

oscillator rather than a flat-bottomed potential is used. However, we are not convinced about the validity of their prescription to derive the renormalization factor.

Let us briefly recall their method. The new feature is to require self-consistency between the deformation coordinates $\varepsilon_\nu^{\text{micr}}$ of the *Strutinsky-smeared* microscopic matter distribution and the deformation coordinates $\varepsilon_\nu^{\text{macr}}$ for which the macroscopic energy is evaluated. This is contrary to the usual prescription which is to put the coordinates $\varepsilon_\nu^{\text{macr}}$ equal to the deformation coordinates $\varepsilon_\nu^{\text{pot}}$ of the potential. While ref. [31]) obtains $\varepsilon_2^{\text{micr}} \sim \varepsilon_2^{\text{pot}}$ they find $\varepsilon_3^{\text{micr}} \sim \frac{1}{2}\varepsilon_3^{\text{pot}}$ (and $\varepsilon_4^{\text{micr}} \sim \frac{1}{2}\varepsilon_4^{\text{pot}}$). Thus, with their prescription with $\varepsilon_3^{\text{macr}} \sim \frac{1}{2}\varepsilon_3^{\text{pot}}$ the macroscopic energy will increase much less rapidly as the potential deforms mass-asymmetrically than in the usual prescription where $\varepsilon_3^{\text{macr}} = \varepsilon_3^{\text{pot}}$. However, in a similar calculation in the Ra region, but with a somewhat different prescription for ensuring self-consistency, we have found that $\varepsilon_3^{\text{micr}} \sim \varepsilon_3^{\text{pot}}$ [ref. [32])].

The macroscopic energy formula in the present work has a surface energy term of the form derived by Krappe, Nix and Sierk [36]) from a saturating Yukawa-plus-exponential force. A physical consequence of taking the finite range of the nuclear forces into account is that the macroscopic energy becomes less sensitive to wiggles on the surface. Therefore it gets softer toward higher multipole deformations in general. Parameters for the various terms of the macroscopic energy were recently determined by Möller and Nix [27]). They reproduce the fission barriers of 28 nuclei with a rms deviation of 1.33 MeV, and the ground-state masses of 1323 nuclei with a rms deviation of 0.835 MeV.

2.2. DETAILS OF CALCULATION

The folded-Yukawa single-particle levels are calculated with a set of "^{226}Ra" parameters [27]):

$$a = 0.8\,\text{fm}, \qquad R = 7.789\,\text{fm},$$
$$V_n = 45.066\,\text{MeV}, \qquad V_p = 59.934\,\text{MeV},$$
$$\gamma_n = 35.74, \qquad \gamma_p = 33.65.$$

The macroscopic Yukawa-plus-exponential energy is calculated with an earlier [36]) set of parameters than those determined in ref. [27]). This inconsistency is not important since the potential-energy difference $\Delta E = E(\varepsilon_3) - E(\varepsilon_3 = 0)$ extracted in the present work is very insensitive to the choice of parameters.

The shapes are defined by Nilsson's ε_ν parametrization [37]) on the three-dimensional lattice:

$$\varepsilon_2 = 0(0.05)0.25,$$
$$\varepsilon_3 = 0(0.04)0.16,$$
$$\varepsilon_4 = -0.12(0.04)0.04.$$

The shapes are made smoother by including the higher multipoles

$$\varepsilon_5 = -0.9\varepsilon_2\varepsilon_3 ,$$

$$\varepsilon_6 = -\varepsilon_4(\varepsilon_2 + 0.1) .$$

Two-dimensional potential-energy surfaces in ε_2 and ε_3 are obtained by minimization with respect to ε_4. A very low energy was obtained for the point at $\varepsilon_2 = 0.104$, $\varepsilon_3 = 0.1$, $\varepsilon_4 = -0.06$, $\varepsilon_5 = 0$, $\varepsilon_6 = 0.01$ for nuclei close to ^{222}Ra in ref. [27]). The calculated energy at this point is used for the ground-state mass in nuclei where it is below the minimum value interpolated from the lattice points.

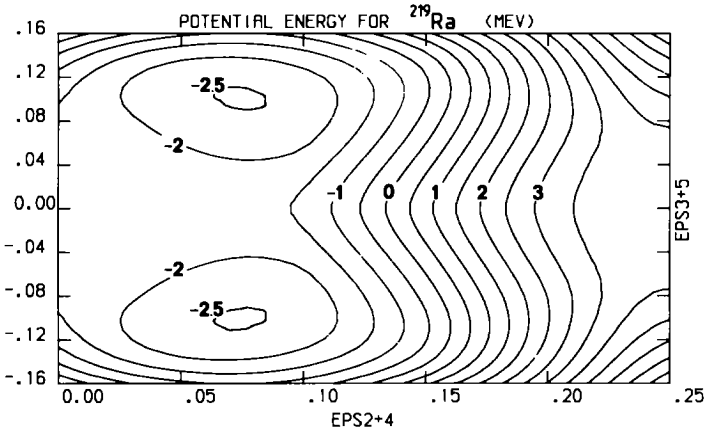

Fig. 1a. Potential-energy surface for ^{219}Ra, calculated by use of a folded-Yukawa single-particle potential and a doubly-folded Yukawa-plus-exponential potential for the surface energy. The ground-state energy is lowered by about 0.8 MeV by the mass-asymmetric shape degrees of freedom. The energy has been minimized with respect to ε_4.

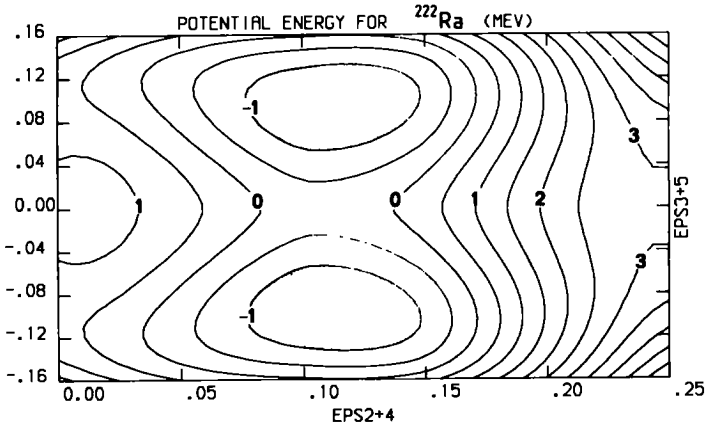

Fig. 1b. Same as fig. 1a, but for ^{222}Ra. The energy is lowered by about 1.2 MeV by the mass-asymmetric shape degrees of freedom. The energy is still lower in a point that is not included in the set of grid-points used to plot the figure (see text for additional details).

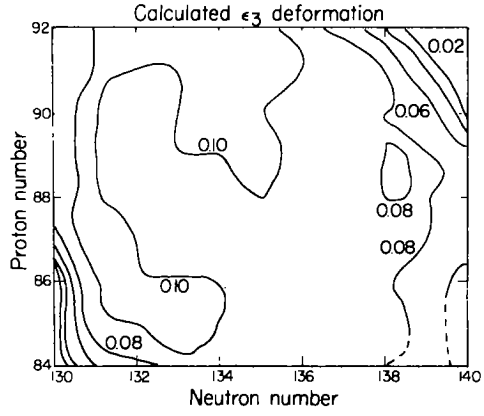

Fig. 2. Calculated ground-state values of the ε_3 deformation coordinate. The values were determined from surfaces of the type exemplified in figs. 1a and 1b.

2.3. RESULTS

Some typical calculated potential-energy surfaces are shown in figs. 1a and 1b. These display the calculated total energy as a function of the deformation coordinates ε_2 and ε_3. Figs. 2 through 4b summarize the results of the potential-energy calculations. Fig. 2 illustrates how a fairly large number of nuclei have ground-state octupole deformations $\varepsilon_3 \sim 0.08$–0.1. There are not many nuclei with smaller but non-zero ε_3 deformation. The existence of well-stabilized octupole minima was known from ref. [27]), and the systematics are examined in sect. 3 below. Here we remark on some further aspects of the results.

The minimal valley in the ε_3 direction follows an almost straight line, $\varepsilon_2 =$ constant, for the deformed cases with $\varepsilon_2 \geq 0.1$ (e.g. fig. 1b). Thus, contrary to ref. [9]),

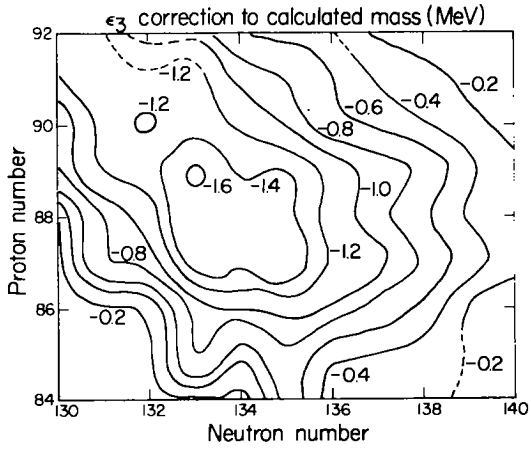

Fig. 3. Calculated correction to the ground-state mass, due to reflection asymmetry. The plot is based on the folded-Yukawa calculation described in the text.

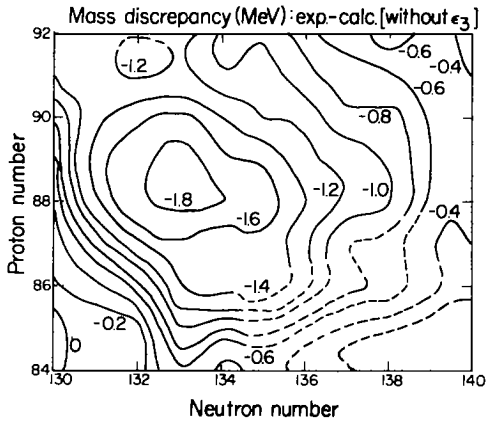

Fig. 4a. Experimental mass minus calculated mass, when only the symmetric shape coordinates ε_2 and ε_4 were considered in the calculations. The dashed contours have been drawn by the plotting code in the regions where there are no experimental data.

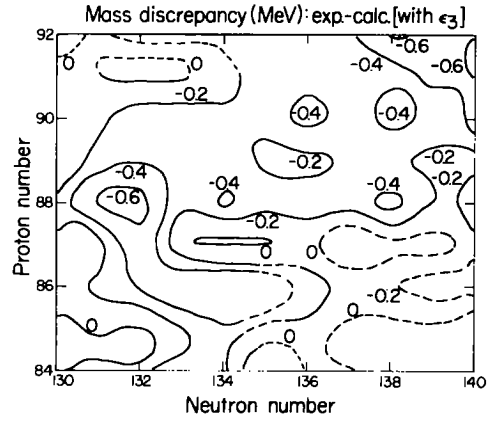

Fig. 4b. Experimental mass minus calculated mass when both symmetric (ε_2 and ε_4) and mass-asymmetric (ε_3) coordinates were considered in the calculations. It is obvious that no large systematic discrepancies remain in this region.

we conclude that the $K = 0$ quadrupole and octupole modes should couple only weakly. For spherical nuclei, however, the two modes appear to be strongly coupled. There is a minimal valley in the potential surface between spherical shape and a shape with $\varepsilon_2 \sim \varepsilon_3 \sim 0.09$. In the transition nuclei where the energy is about the same for these two shapes there may even be a low saddle in between, although it is hard to distinguish with the present lattice. Such a potential suggests a dynamical shape coexistence, which may help to explain for example why the observed moment of inertia of the $K^\pi = 0^-$ band is almost constant while the moment of inertia of the ground band decreases sharply for N below 132 [ref. [38])]. Notably, at higher

spins, the yrast band in the transitional nucleus ^{218}Ra is one of the few cases where the energy levels have alternating even and odd parity [39]) [another [40]) is ^{152}Dy].

In the deformed cases there is a large negative equilibrium value of ε_4, corresponding to a large positive hexadecapole moment. The minimal value of ε_4 does not depend very sensitively on ε_3. Typically the absolute value is about 10% lower in an octupole deformed minimum than on the $\varepsilon_3 = 0$ saddle.

For a number of nuclei around ^{222}Ra, the calculated potential-energy gain relative to the lowest symmetric shape is more than 1 MeV (figs. 1a, 1b and 3). If this is true for real nuclei the reflection asymmetric deformation must be regarded as stable rather than dynamical because the $K^\pi = 0^-$ excitation energy in these nuclei is known to be 0.2–0.3 MeV, considerably smaller than the symmetric barrier between the mirror images. This criterion for stability of the octupole deformation is based on the plausible assumption that the zero-point energy contribution in the ground state from tunneling through the barrier is not much larger than the energy of an octupole excitation – simple models suggest it should lie within a factor of about 2. Thus, when the barrier at $\varepsilon_3 = 0$ is much larger than this energy, it follows that the amplitude of the ground-state wave function at $\varepsilon_3 = 0$ is small. It is in principle possible that a lower barrier between the $K = 0$ mirror images can be found along another path in deformation space. This would not necessarily detract from the stability of the reflection asymmetry, by the same token that γ-instability does not detract from the stability of β-deformation.

The $K^\pi = 1^-, 2^-, 3^-$ band heads are located at or above ~1 MeV, and individually they presumably have a vibrational character with respect to the $K = 0$ octupole deformed ground state. These higher bands mix considerably through the Coriolis interaction with the rotational states of the $K = 0$ band [28,35,41]), and it is not obvious what the implications might be for the stability of reflection asymmetry at higher spins. To understand the interaction among the full quadrupole, octupole, rotational, pairing and single-particle degrees of freedoms is a challenging field of future research.

3. Masses

The Möller–Nix nuclear masses calculated without the octupole degree of freedom [27,42]) show large deviations from experiment around ^{222}Ra (fig. 4a). The deviations occur in precisely the same nuclei where the calculated potential-energy minimum is lowest for a reflection asymmetric shape (fig. 3). When the octupole effect is taken into account the systematic discrepancy between theory and experiment goes away (fig. 4b). The remaining discrepancy over this mass region is small compared to the rms deviation of the mass formula.

These results strongly support the interpretation that nuclei in this region have a stable octupole deformation in their ground state. Since an effect of 1–2 MeV could not come from the changes in a vibrational zero-point energy for these nuclei,

there is good reason to believe that the octupole effect is accurately described by the calculations.

The corresponding extension of the mass table of ref. [42]) is obtained by adding the ΔE of fig. 3 to the calculated mass excess values of ref. [42]).

4. Spectroscopy of doubly even nuclei

In this section we revisit the description of the low-lying $K = 0$ octupole excitations in terms of one-dimensional collective motion with the hamiltonian

$$H = H_0 - \frac{\hbar^2}{2B}\frac{\mathrm{d}^2}{\mathrm{d}\varepsilon_3^2} + V(\varepsilon_3)\,.$$

Some different possibilities are shown schematically in fig. 5. The collective potential V is necessarily symmetric around $\varepsilon_3 = 0$, so the solutions have alternating parity. For symmetry reasons the odd-spin states are absent in rotational bands based on the positive-parity solutions, while even-spin states are absent for negative parity. When there is a very high barrier between a reflection asymmetric shape and its mirror image, the $0^+, 1^-, 2^+, \ldots$ sequence is expected to form a single band. When the barrier is lower, a tunneling between the mirror shapes gives rise to a displacement of two bands of opposite parity, i.e. $I^\pi = 0^+, 2^+, 4^+, \ldots$ and $I^\pi = 1^-, 3^-, 5^-, \ldots$, with even spins favored energetically. For a double oscillator the amount of displacement, or parity splitting, is easily obtained in perturbation theory [43]). As the barrier disappears entirely the spectra go smoothly over into the octupole vibrational limit (fig. 5).

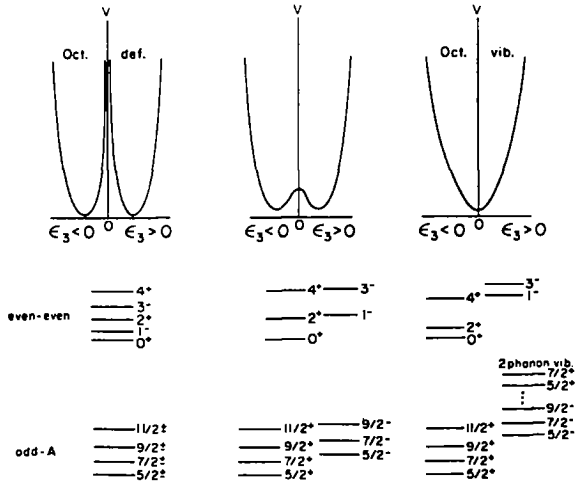

Fig. 5. Schematic picture of how a rotational band is expected to depend on the potential energy for $K = 0$ reflection asymmetric deformation.

The potential curves obtained from the calculations of sect. 2 above are specified in table 1, which shows the energy for $\varepsilon_3 = 0$ and $\varepsilon_3 = 0.16$, relative to the ground-state minimum. Also tabulated are the ground-state shape coordinates. We note in particular that the calculated value of ε_3 at the ground-state minimum of ^{226}Ra is in agreement with recent experimental data. The calculated value, $\varepsilon_3 = 0.08$, can

TABLE 1

Properties of the calculated potential-energy minimum for selected doubly even nuclei

Z	A	$E(\varepsilon_3=0) - E(\varepsilon_3^{\min})$ (MeV)	$E(\varepsilon_3=0.16) - E(\varepsilon_3^{\min})$	$\varepsilon_2^{\min}$	$\varepsilon_3^{\min}$	$\varepsilon_4^{\min}$
84	218	0.10	1.75	0.045	0.087	−0.019
	220	0.32	1.45	0.075	0.087	−0.035
86	218	0.23	1.60	0.059	0.100	−0.030
	220	0.81	1.59	0.091	0.100	−0.048
	222	0.95	1.64	0.109	0.093	−0.054
	224	0.48	1.48	0.139	0.080	−0.062
	226	0.12	1.66	0.152	0.053	−0.066
	228	0.01	2.37	0.175	0.007	−0.063
88	220	1.02	1.59	0.091	0.093	−0.051
	222	1.46	1.81	0.111	0.093	−0.060
	224	1.01	1.42	0.134	0.093	−0.062
	226	0.69	1.63	0.150	0.080	−0.068
	228	0.17	1.71	0.164	0.067	−0.066
	230	0.01	2.33	0.186	0.007	−0.066
	232	0.01	2.80	0.198	0.013	−0.059
	234	0.02	3.16	0.209	0.013	−0.048
90	220	0.52	1.83	0.075	0.093	−0.035
	222	1.36	1.70	0.102	0.093	−0.053
	224	1.20	1.27	0.130	0.100	−0.058
	226	0.67	1.31	0.150	0.093	−0.061
	228	0.28	1.53	0.161	0.080	−0.067
	230	0.04	1.86	0.182	0.013	−0.074
	232	0	2.72	0.195	0	−0.071
	234	0	3.13	0.202	0	−0.063
	236	0.01	3.33	0.211	0.007	−0.053
92	222	0.95	1.84	0.086	0.093	−0.035
	224	1.09	1.68	0.116	0.100	−0.049
	226	0.54	1.33	0.143	0.100	−0.055
	228	0.17	1.53	0.155	0.093	−0.059
	230	0	2.07	0.184	0	−0.080
	232	0	2.75	0.193	0	−0.077

Columns 1 and 2 indicate the nucleus. Column 3 shows the energy, relative to the minimum, obtained by minimization for reflection symmetric shapes only. Column 4 gives the relative energy of the lowest point along the line $\varepsilon_3 = 0.16$, which is useful in defining a one-dimensional potential-energy curve as a function of ε_3. Columns 5–7 indicate the minimal shape. Values for ε_5 and ε_6 are prescribed in subsect. 2.2.

be translated through the formula

$$B(\mathrm{E3}) = \frac{7}{16\pi} Q_{30}^2 \langle I_i K_i 30 | I_f K_f \rangle^2 ,$$

where

$$Q_{30} = -\tfrac{6}{7} Z R_0^3 \varepsilon_3 ,$$

into a transition rate, $B(\mathrm{E3}; 0^+ \to 3^-) \approx 0.7 e^2 \cdot \mathrm{b}^3$, which should be compared to the experimental value $0.74 \pm 0.04 e^2 \cdot \mathrm{b}^3$ inferred from Coulomb excitation measurements by the Munich group [29]).

The information on the potential in table 1 fixes a, C and D in a parametrization of the form

$$V(\varepsilon_3) = \tfrac{1}{2} C \varepsilon_3^2 + D(\mathrm{e}^{-\varepsilon_3^2/a^2} - 1) .$$

Fig. 6 shows numerical solutions in a sequence of such potentials with $C = 200$ MeV and a deformed minimum at $\varepsilon_3 = 0.08$. The quantity V_0 on the abscissa of fig. 6 is

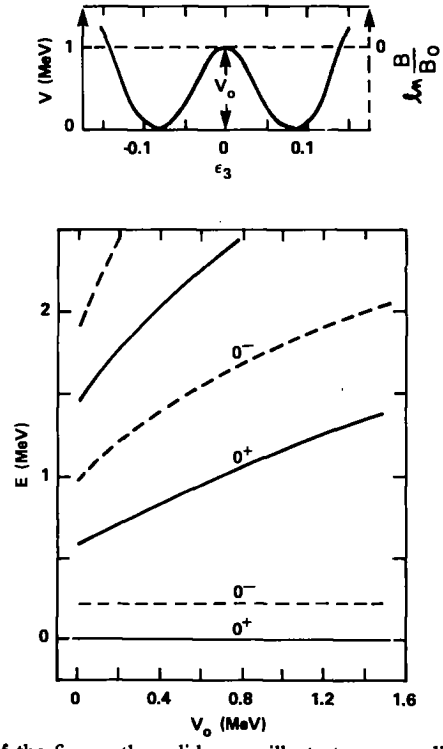

Fig. 6. In the upper part of the figure, the solid curve illustrates a one-dimensional potential-energy curve with $V_0 = 1$ MeV, while the horizontal dashed line indicates a constant inertial mass. The lower part of the figure shows the eigenstates for one-dimensional motion as a function of the parameter V_0. In rotational nuclei these states would correspond to band heads, though for negative parity the 0^- level would be missing so the 1^- level would be the lowest actually occurring band member. For each V, the inertial mass constant is adjusted so that the lowest 0^- excitation comes at 238 keV, a value appropriate for the radium region.

the height of the barrier at $\varepsilon_3 = 0$ relative to the potential minimum. The inertial mass B is taken to be a constant whose value is adjusted so that the 1^- level in each case comes at 250 keV, including a rotational energy computed with $\hbar^2/2\mathcal{I} =$ 6 keV. From fig. 6 it is seen that the non-observation [28]) of any excited 0^+ states below 900 keV in the nuclei ^{224,226}Ra implies that the potential barrier at $\varepsilon_3 = 0$ must be at least 0.5 MeV. This is compatible with the calculated barriers in table 1.

It is interesting to see how much this conclusion might be affected if the inertial mass is not constant but depends on ε_3. To this end, the inertial-mass function is parametrized as

$$B = B_0(1 - G\,\mathrm{e}^{-\varepsilon_3^2/f^2})^{-4},$$

a form which becomes convenient for numerical diagonalization in a harmonic oscillator basis after the application of Pauli's quantization formula. If G is positive, B is largest for $\varepsilon_3 = 0$. If G is negative, B has a minimum for $\varepsilon_3 = 0$. The spectrum is shown as a function of G in fig. 7 for the case of a harmonic oscillator potential. The parameters are $B_0 = 200\ \mathrm{MeV}^{-1}$, $C = 200$ MeV and $f = 0.05$, the rms value of ε_3 for $G = 0$. In fig. 7 the energy ratio between the first and second excited states is seen to depend only weakly on the form of the mass function. The same is true also when there is a barrier V_0 at $\varepsilon_3 = 0$.

It remains to be seen whether microscopically calculated inertial-mass functions have a reasonable magnitude [44]).

5. Spectroscopy of odd-A nuclei

5.1. PARITY SPLITTING

The simplest model of an odd-A spectrum in a deformed nucleus is that of a quasiparticle in a single Nilsson orbital [45]). Neutron single-particle orbitals in the Ra region, calculated for comparison in both the modified oscillator and folded-Yukawa models, are given as functions of ε_3 in fig. 8. In the intrinsic frame a $K = 0$ octupole deformation conserves Ω, chosen as $\frac{5}{2}$ in fig. 5, but not the parity. For a stable octupole deformation one then expects a $K = \Omega$ rotational band with doubly degenerate states of the same spin but opposite parity. For an octupole vibration around a reflection asymmetric shape, however, one would use a Nilsson orbital of good parity corresponding to the symmetric shape. The odd-A ground band has that parity, while states of opposite parity may be obtained by a $K = 0$ one-phonon octupole vibration. The energy splitting between states of the same spin but opposite parity is equal to the octupole phonon energy, which in the doubly even case is obtained by extrapolating the negative-parity band down to the missing 0^- band head.

In order to relate to experiment, it is necessary to identify the parity doublets in the observed spectra. This has been done very tentatively for a few nuclei in

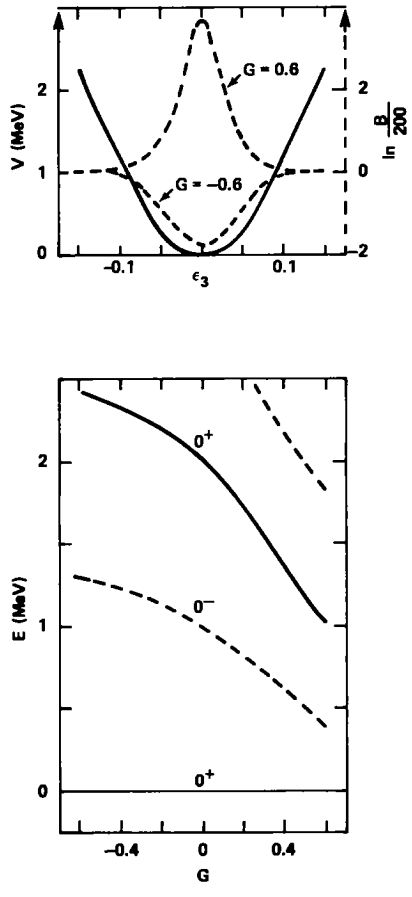

Fig. 7. Similar to fig. 6, but the potential is a fixed parabola and the levels in the lower part of the figure are plotted as a function of a parameter G, which determines the functional form of the inertial mass function. Positive and negative G-values correspond to very large and very small masses, respectively, near the center of the potential well, as indicated by two dashed curves in the upper part of the figure.

table 2. It turns out that the parity splitting in the odd-A nuclei is consistently smaller by about 150 keV than the parity splitting in their doubly even neighbours (fig. 9). The reduction of the parity splitting for each is indicated in column 7 of table 2, where it is referred to as the "specialization energy" due to the presence of the odd particle. In the following two parts of this section we first consider shape polarization due to the odd particle as a possible explanation and then proceed to develop a still simple but more adequate picture of the interaction between collective and single-particle degrees of freedom.

TABLE 2

Octupole separation energies and specialization energies for Nilsson orbitals in odd-A nuclei

1 Nucleus	2 Orbital	3 Energy (keV)	4 Opposite parity energy (keV)	5 ΔE_{oct} (keV)	6 Even–even ΔE_{oct} (keV)	7 6–5 specialization energy (keV)	8 $\hbar^2/2\mathcal{I}$ (keV)	9 $\hbar^2/2\mathcal{I}$ opposite parity (keV)	10 Comments
$^{223}_{89}$Ac	$\frac{5}{2}^-[523]$	0	65	65	227.0	162.0			g.s. band spins and parities not certain, but parities of 65 keV band opposite
$^{225}_{89}$Ac$_{136}$	$\frac{3}{2}^-[532]$	0	40	40	201.2	161.2			g.s. band parities not certain, but parities of 40 keV band opposite
	$\frac{5}{2}^-[523]$	120.8	155.5	34.7	201.2	166.5	7.11	6.34	spins and parities of bands tentative
$^{227}_{88}$Ra	$\frac{1}{2}^+[631]$	120.7	296.6	175.9	240.2	64.3	8.32		decoupling parameters have opposite signs as expected
	$\frac{5}{2}^+[633]$	1.7 [a])	475.0 (?)	473.3	240.2	−244.1	5.14		
$^{227}_{89}$Ac$_{138}$	$\frac{3}{2}^-[532]$	0	27.4	27.4	240.2	212.8	6.18	4.77	$\hbar^2/2\mathcal{I}$ quite different for the two bands
	$\frac{1}{2}^-[530]$	354.6	435.3	80.9	240.2	159.3	10.4	12.7	band sequences quite different; decoupling parameters have opposite signs as expected
$^{229}_{90}$Th$_{139}$	$\frac{5}{2}^+[633]$	0	146.4	146.36	314.4	168.0	6.06	6.0 [b])	
	$\frac{3}{2}^+[631]$	0	164.5	164.5	314.4	149.9	5.84	6.0 [b])	
$^{231}_{90}$Th	$\frac{5}{2}^+[633]$	0	185.7	185.7	495.5	309.8	6.0	2.8	very different $\hbar^2/2\mathcal{I}$ doubtful
$^{233}_{91}$Pa	$\frac{1}{2}^-[530]$	6.7	169.2	162.5	772.3	609.8	8.0	5.4	opposite sign for decoupling parameters; very different $\hbar^2/2\mathcal{I}$
$^{233}_{92}$U	$\frac{5}{2}^+[633]$	0	298.0	298.0	550.0	252.0	5.8	3.1	

[a]) This octupole state is considered to be a mixture of two octupole states and is therefore anomalous.

[b]) Inverse moments of inertia ($\hbar^2/2\mathcal{I}$) are those used by Kroger and Reich [47]) as input parameters in Coriolis coupling to reproduce experimental spectrum.

Column 5 gives the energy of separation between the states of the same spin but opposite parity for the orbitals listed in column 2. Column 6 gives the same energy of separation for the even–even core, assumed here to be the core with one less nucleon and with the rotational zero-point energy subtracted. The difference between column 6 and column 5, which is the specialization energy, is listed in column 7. Data for this table are from von Egidy *et al.* [46]) for ^{227}Ra and from Nucl. Data and the Table of Isotopes.

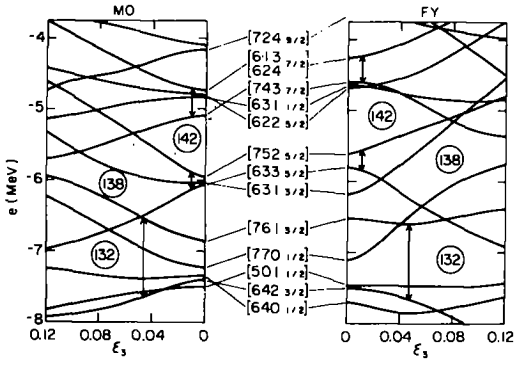

Fig. 8. The single-neutron orbitals plotted versus octupole deformation, ε_3, in a modified oscillator potential (left) and a folded-Yukawa potential (right). The other deformation coordinates are defined by $\varepsilon_2 = 0.15$, $\varepsilon_4 = -0.054$ and $\varepsilon_2 = 0.16$, $\varepsilon_4 = -0.08$, respectively, corresponding approximately to the equilibrium values for ^{226}Ra in the two different potentials. The states for $\varepsilon_3 = 0$ are labelled by the largest $[Nn_z\Lambda\Omega]$ component. Some orbitals which couple strongly through the Y_{30} operator are connected by arrows.

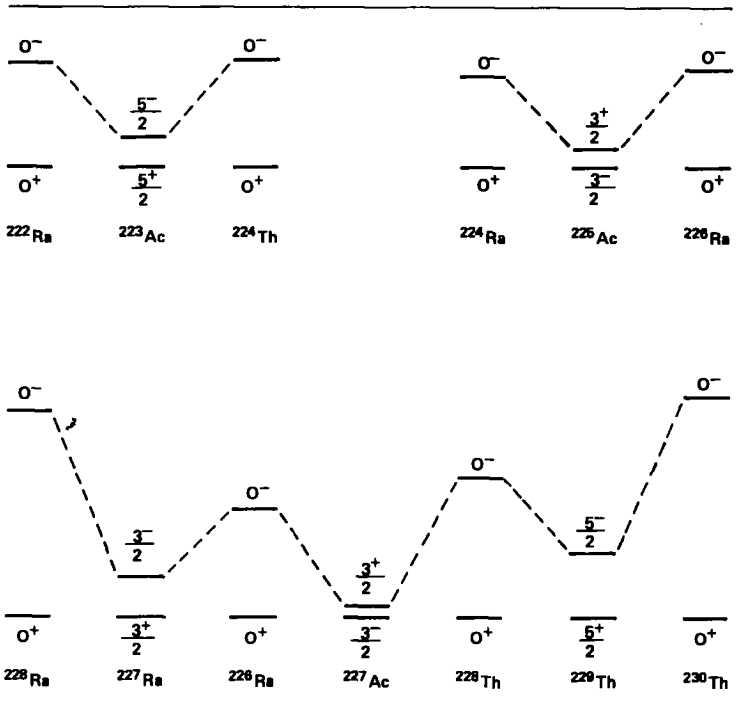

Fig. 9. Experimental ground states and parity conjugates, tentatively assigned in table 2, are plotted so as to illustrate the relation between odd-A nuclei and their doubly even neighbours.

5.2. POLARIZATION

It is well known that a quasiparticle in a specific Nilsson orbital polarizes the nuclear shape in such a way that this orbital comes closer to the Fermi level. The driving force is proportional to the slope of the orbital in a Nilsson diagram. Fig. 8 shows the Nilsson diagram in the octupole ε_3 coordinate at the ε, ε_4 deformation relevant e.g. for the well-studied nuclei ^{227}Ra [ref. [46])] and ^{229}Th [ref. [47])]. The Nilsson levels are seen to be very similar in the folded-Yukawa and modified oscillator potentials, the latter of which was used for the numerical calculations of this subsection. The $K = \frac{5}{2}$ orbitals nearest the Fermi level for $N = 139$ slope *away* from the Fermi level for $\varepsilon \leq 0.1$, the nearest $K = \frac{1}{2}$ and $K = \frac{7}{2}$ orbitals slope *toward* it while the $K = \frac{3}{2}$ level is neutral. The magnitude of the quasiparticle effect is shown in fig. 10, where potential-energy curves along the respective minimal valleys in the ε_3 direction are shown for different quasiparticle configurations of ^{227}Ra. To obtain the total energy for the odd nucleus, the macroscopic contribution and the shell energy have been calculated in the same way as for an even nucleus. Then the pairing+specialization energy was added. Two approaches are possible. In the

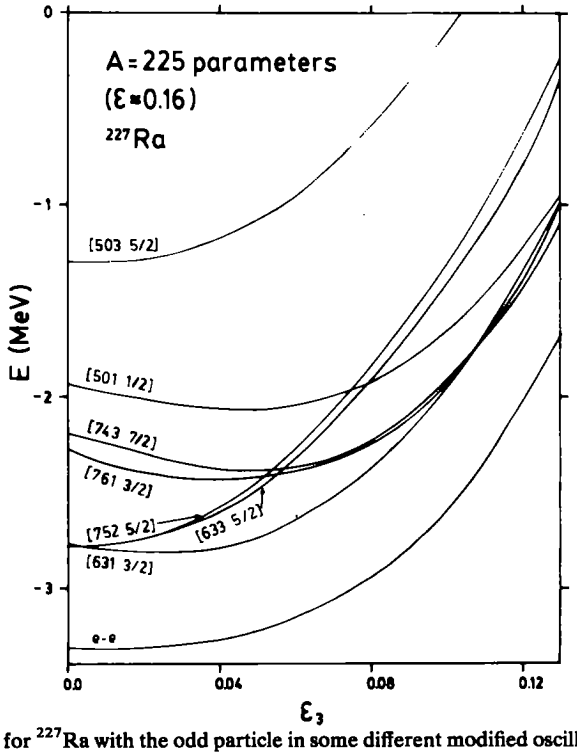

Fig. 10. The energy for ^{227}Ra with the odd particle in some different modified oscillator orbitals, plotted as a function of ε_3. The curve labelled "e–e" shows the calculated mean value between ^{226}Ra and ^{228}Ra. The energy has been minimized with respect to ε_2, which in all cases stays close to 0.16. The orbitals of the two curves labelled [752 $\frac{5}{2}$] and [633 $\frac{5}{2}$] are strongly mixed. Note however that one is rather of hole character while the other is of particle character.

one used here the pairing equations are solved with the orbital, ν, of the odd particle blocked. The single-particle energy of the odd particle, $e_\nu - \lambda$, is added to the resulting energy. Here, λ denotes the calculated Fermi energy. The alternative procedure of solving the BCS equations without blocking and subsequently adding the quasiparticle energy $E_\nu = \sqrt{(\varepsilon_\nu - \lambda)^2 + \Delta^2}$ was found to give approximately the same specialization energy. The even–even reference curve in fig. 10 is also evaluated with a modified-oscillator potential, which gives a smooth up-slope, but relative to the reference the single-particle effects would of course be similar in the folded-Yukawa model.

The potential energy at $\varepsilon_3 \sim 0.1$, relative to the potential energy at $\varepsilon_3 = 0$, is raised or lowered by about 0.5 MeV depending on whether the quasiparticle has $K = \frac{5}{2}$ or $\frac{7}{2}$, respectively. This should have a significant effect on the tunneling matrix element, in the folded-Yukawa description where there is a barrier, and thus on the parity splitting. However, it is hard to understand the tentative empirical observation in table 2 and fig. 9, that the parity splitting always goes down by about 150 keV in odd-mass nuclei.

5.3. FRAGMENTATION

The procedure adopted above of placing the odd particle in one Nilsson orbital, should be most accurate for large deformations. For small deformations, however, it does not generally give a good description, and in particular for small ε_3 deformation the broken reflection symmetry may not be properly accounted for.

In fig. 8 there are numerous examples of orbitals with the same Ω, which at $\varepsilon_3 = 0$ have opposite parity and come close in energy. This is no coincidence. It is precisely these orbitals which interact strongly through a Y_{30} term and thereby help to sustain it. In the following we describe a simple model for odd-mass nuclei with octupole deformation, which takes into account both of these interacting single-particle orbitals.

The single-particle space is shown to the left in fig. 11. It is spanned by two Nilsson orbitals with the same Ω, opposite parities and single-particle energies $-\varepsilon$

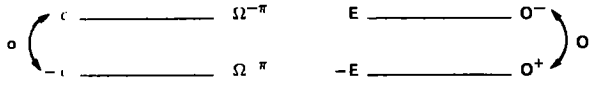

Fig. 11. An exactly solvable particle-core coupling model. The particle may occupy either of the two Nilsson orbitals on the left, and the core may be in either of the two K-bands on the right. The interaction term to be diagonalized is κoO.

and ε, respectively. The matrix element of the single-particle octupole operator between them is o. Similarly the core space to the right in fig. 11 has two levels with K^π equal to 0^+ and 0^-, respectively, connected by a collective octupole matrix element O. The absence of higher-lying vibrational states in the core corresponds to a relatively stable octupole shape. The core-particle coupling hamiltonian can be written

$$H = H_{\text{core}} + H_{\text{part}} + V$$

in the four-dimensional space spanned by the four possible combinations of particle and core states where the off-diagonal core-particle matrix elements are

$$V = \kappa o O .$$

Since H is block diagonal, with two 2×2 blocks corresponding to the total parities π and $-\pi$, respectively, it is trivial to diagonalize. The expression for the parity-splitting between the lowest eigenstates of this schematic odd-A system is

$$e_<^{-\pi} - e_<^{\pi} = \sqrt{(E+\varepsilon)^2 + V^2} - \sqrt{(E-\varepsilon)^2 + V^2} .$$

From this expression it is straightforward to show that *there is always a reduction of the parity splitting in the odd-A case* relative to the even-A case. For example, if $V = E = \varepsilon$ the parity splitting is reduced from $2E$ to $(\sqrt{5}-1)E$, and if $V = E \gg \varepsilon$ it becomes $\sqrt{2\varepsilon}$. The parity splitting of the core states is empirically $2E \sim 0.3$ MeV in the radium region, the core-particle octupole–octupole interaction from the folded-Yukawa calculation is $V \sim 1$ MeV, and the splitting between appropriate single-particle levels in the Nilsson scheme for reflection symmetric shapes, 2ε, may be anywhere in the range from 0 to about 1 MeV (fig. 8). Inserting these numbers into the formula above, it becomes clear that the magnitude of the reduction is compatible with the experimental values in table 2.

The underlying mechanism for the reduction has a different character depending on whether the separation between the Nilsson orbitals, 2ε, is smaller or larger than the even-A parity splitting, $2E$. If $\varepsilon < E$, the total parity splitting becomes even smaller than the single-particle separation, corresponding to the fragmentation of some collectivity onto a primarily single-particle mode. However, when the single-particle separation is larger than the parity splitting of the even core, $\varepsilon > E$, the reduction of the parity splitting in the odd-A system should probably be characterized as polarization, with the single-particle mode contributing coherently to the collective mode. A manifestation of this is that, for $\varepsilon > E$, there is a reduction of the parity splitting only if the particle–core octupole–octupole interaction V is non-zero.

The considerable reduction of the parity-splitting observed in the Ra-Ac-Th region (fig. 9) suggests that the primary mechanism in most of these cases is fragmentation. This is also plausible in view of the calculated single-particle levels (fig. 8). The active pairs of Nilsson orbitals at $\varepsilon_3 = 0$ come even closer when pairing

is taken into account and quasiparticle energies are employed. The amount of fragmentation can be measured directly in terms of the E3 transition rate between the two low-lying states of opposite parity in the odd-mass nucleus. Fragmentation would reduce the E3 rate below that in the doubly even neighbors by an amount that is straightforward to calculate in the exactly solvable model of fig. 11. Calculations based on a related but more realistic model are in progress [44]). Previously, Chasman has noted a considerable variation between different nuclei in the B(E3) rates resulting from his calculations [30]). A preliminary report on B(E3) measurements in odd-A nuclei was recently presented by Ahmad *et al.* [48]).

In summary, the following four quantities could give insight into the octupole structure of an individual odd-A nucleus:

(i) parity splitting of even-A core – relates to E,

(ii) parity splitting of odd-A nucleus – relates to ε,

(iii) B(E3) in even-A core – relates to ε_3,

(iv) B(E3) in odd-A nucleus – tests validity of a theoretical value of V and the effect of additional basis states which may be included in the coupling calculation.

6. General features of the octupole favoring shell effects

With the investigation of the octupole degree of freedom in the Ra/Th region as a background we will devote this section to a more general discussion of shell effects as a function of octupole deformation and particle number. For this purpose, figs. 12–14 were prepared. For deformation $\varepsilon = 0$ and ± 0.2, the neutron shell

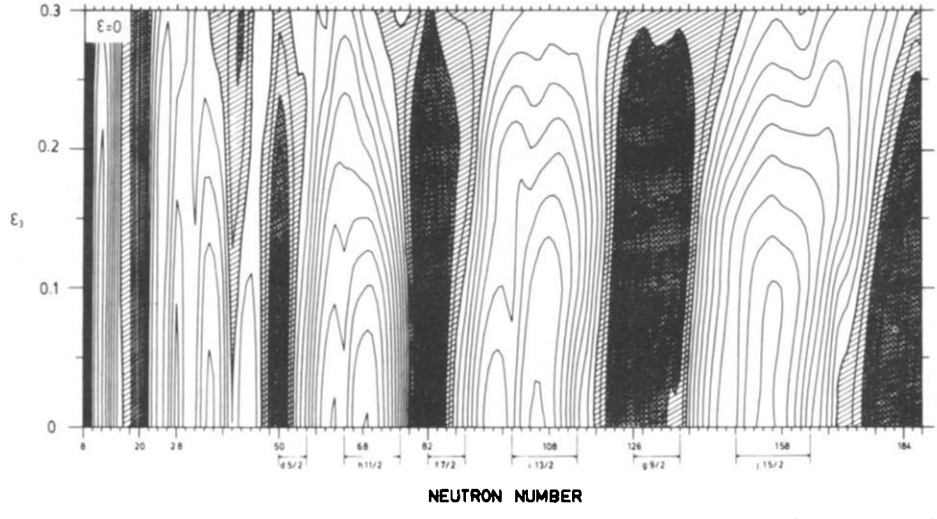

Fig. 12. The neutron shell energy landscape for $\varepsilon_2 = \varepsilon_4 = 0$ plotted as a function of neutron number and octupole deformation, ε_3. The heavy lines separate regions of positive and negative shell energy. In the heavy-shaded regions, the shell energy is smaller than -2 MeV. The neutron numbers of the subshells which couple strongly through the Y_{30} term are indicated.

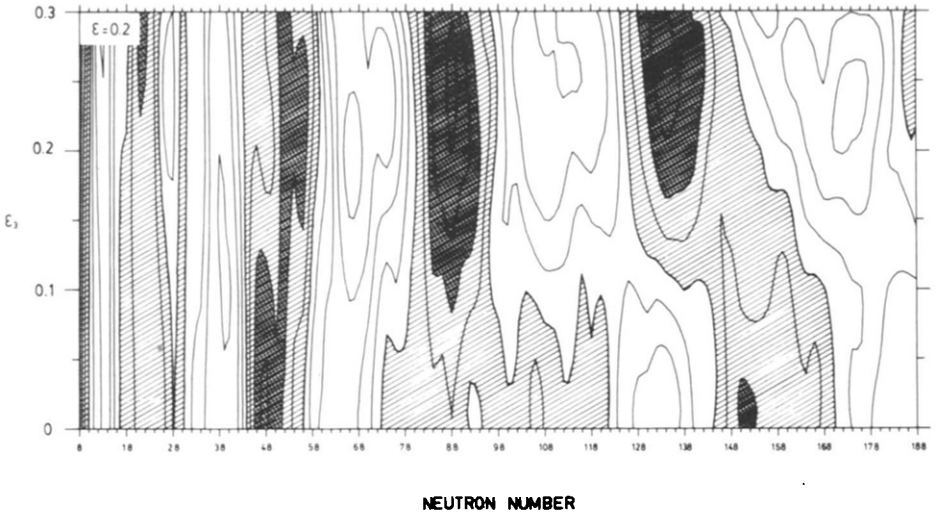

Fig. 13. Same as fig. 12 but for $\varepsilon_2 = 0.2$ ($\varepsilon_4 = 0$).

energy is plotted as a function of deformation ε_3, and neutron number N. The Nilsson model has been used with different κ- and μ-values for different shells [49,50]). The corresponding single-particle diagram is presented in ref. [51]).

It is well known that for spherical shapes (fig. 12) it is mainly orbitals of the type $|Nlj\rangle$ and $|N+1l+3j+3\rangle$ which couple strongly through the Y_{30} term. Such orbitals come close to each other when the high-j intruder shell comes down into the N-shell below. This happens for medium-heavy and heavy nuclei and is associated with the 3:1 shell structure discussed in subsect. 2.1. The best example seems to be the

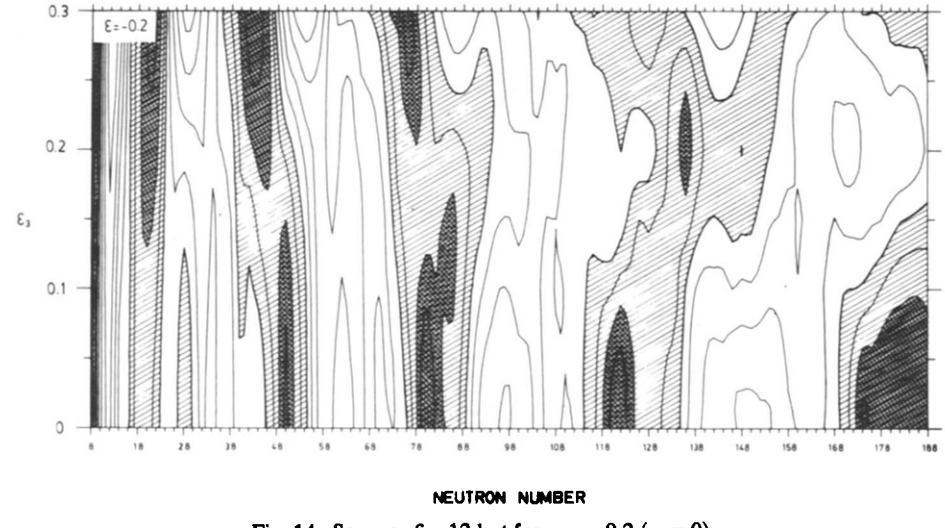

Fig. 14. Same as fig. 12 but for $\varepsilon_2 = -0.2$ ($\varepsilon_4 = 0$).

interaction between $g_{9/2}$ and $j_{15/2}$ for $N > 126$. These subshells are quite close in energy for spherical shape. The particle numbers where these orbitals are being filled are indicated along the bottom of fig. 12. One observes that the simple picture is somewhat obscured by the fact that the $i_{11/2}$ subshell comes in between $g_{9/2}$ and $j_{15/2}$. Even so, the shell energy for the spherical system at for example $N = 136$ decreases by ~ 3 MeV when ε_3 goes from 0 to 0.15. Also for other neutron numbers below the start of the $j_{15/2}$ shell ($N = 148$), similar effects of ε_3 are observed. The single-particle mechanism behind this shell energy decrease is that the $g_{9/2}$ and $j_{15/2}$ orbitals repel each other with increasing ε_3. This leaves a region of lower level density between these two subshells. (This is the general shell energy response when specific orbitals couple through some operator which in this case is $r^2 Y_{30}$.)

Some other subshells which also interact via the $r^2 Y_{30}$ operator are indicated at the bottom of fig. 12. These are the $f_{7/2}$ and $i_{13/2}$ shells for $N \simeq 82$, $d_{5/2}$ and $h_{11/2}$ for $N \simeq 50$. The energy spacing between the interacting subshells does, however, increase with decreasing particle number. Still rather strong shell effects favoring octupole shapes are observed not only in the $N \simeq 140$ region but also in the $N \simeq 90$–100 region and possibly in the $N \simeq 60$ region.

When the nucleus gets deformed the high-j subshells split and the $r^2 Y_{30}$ operator couples the orbitals of for example $g_{9/2}$ and $j_{15/2}$ having the same value of Ω. As these interactions occur at different energies for different Ω, one might expect more diffuse shell effects in the ε_3 direction. However, the calculations at $\varepsilon = \pm 0.2$ show that the variation of shell energy as a function of ε_3 is about as pronounced as for $\varepsilon = 0$. This may be explained by the fact that for deformed shapes, some interacting orbitals come very close to each other (fig. 8). For $\varepsilon = 0.2$, octupole shapes are specifically favored for $N \simeq 86$–90 and $N \simeq 130$–138. For $\varepsilon = -0.2$, the favored neutron numbers are higher, $N \simeq 90$–98 and $N \simeq 138$–152. The decrease of favored neutron numbers when the nuclear shape changes from oblate over spherical to prolate appears to be connected with the fact that the orbitals which are important in creating octupole shapes are mainly those with low or intermediate Ω-values. These orbitals come down in energy for prolate deformations and go up for oblate deformations.

The subshells which are mainly responsible for the octupole favoring shell effects should not be strongly affected by for example ε_4 deformations or use of nuclear models other than the Nilsson model. Thus, the features of limited and well-defined regions of particle numbers where octupole deformations are favored should be of general nature. Furthermore, these regions should be about the same for protons as for neutrons. The variation of the favored regions with quadrupole deformation ε is also expected to be a general feature of nuclear structure.

Finally, let us look at the systematics from available experimental spectroscopy. Data on the energy of the lowest negative-parity excited state known in nuclei from $_{30}$Zn to $_{94}$Pu are compiled in the form of contour plots in figs. 15a–c. The most pronounced minimum occurs in the $_{88}$Ra region discussed above (fig. 15c).

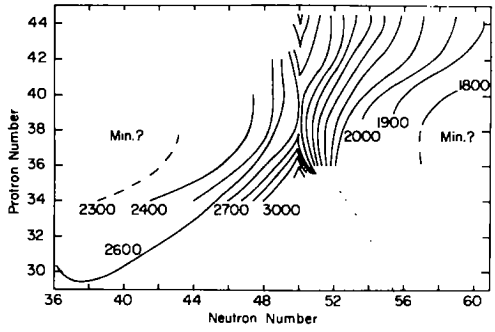

Fig. 15a. The lowest negative-parity energy level in keV, observed experimentally for doubly even nuclei in the range $30 \leq Z \leq 44$, $36 \leq N \leq 60$.

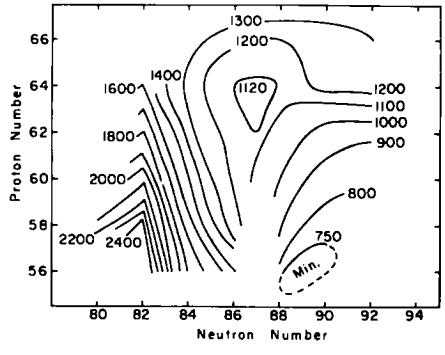

Fig. 15b. Same as fig. 15a, but for $56 \leq Z \leq 66$, $80 \leq N \leq 94$. Recent data in the barium region are from refs. [52,53]).

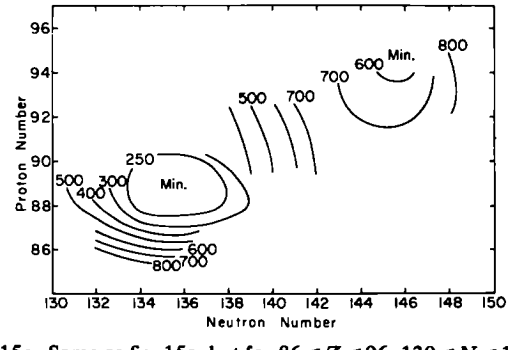

Fig. 15c. Same as fig. 15a, but for $86 \leq Z \leq 96$, $130 \leq N \leq 150$.

There is also a secondary minimum along the β stability line for the heaviest elements. Collective modes are most likely to be adiabatic in heavy nuclei, which makes spectroscopic studies around these two minima in fig. 15c a fruitful prospect. Another challenge is to study the best cases for octupole collectivity in medium mass regions. Figs. 15a, b indicate that the best cases occur just within the limits of stability, for the very neutron-rich $_{56}$Ba region and furthermore the $_{38}$Sr region at both very small and very large neutron numbers. Indeed, in the very limited calculation of ref. [27]) it was found that the nucleus $^{91}_{36}$Kr was very soft with respect to octupole deformations. This was also the nucleus for which the largest discrepancy between calculated and experimental masses occurred. The calculated ground-state energy was too high by 2.87 MeV.

7. Conclusions

It has been realized for some time that the tendency towards instability with respect to one deformation coordinate or another depends on very general principles. This tendency is a function of particle number and deformation and is similar in different models.

The tendency towards instability may show up either as a softness with respect to the deformation coordinate, ε_ν, or as a potential energy minimum for $\varepsilon_\nu \neq 0$. In the macroscopic–microscopic model, this depends on the detailed balance between shell structure, Coulomb energy and surface energy.

In the present investigation we have studied the octupole degree of freedom at the nuclear ground state, in particular for nuclei in the Ra region. The calculations exhibit, contrary to most earlier investigations, substantial octupole instabilities around ^{222}Ra. The reason why we obtain a different result seems to be that we have used a folded-Yukawa single-particle potential contrary to earlier calculations which employ a modified oscillator. It turns out that the important matrix elements of the interaction due to the ε_3 deformation are weaker in the latter single-particle potential.

There are a variety of experimental data that support the theoretical results of parity-mixed intrinsic states. In particular, the inclusion of the octupole degree of freedom in the present calculation gives much better agreement between calculated and experimental masses. Spectroscopic measurement for the $B(\mathrm{E3}: 0^+ \rightarrow 3^-)$ transition rate for ^{226}Ra agrees with the calculated value $\varepsilon_3 = 0.08$ for the ground-state shape. The non-observation of excited 0^+ states below 900 keV in some Ra nuclei implies a barrier of at least 0.5 MeV between the left–right and right–left asymmetric minima. This is compatible with the calculated values. The reduction in parity splitting that is observed in odd-mass nuclei compared to even-mass nuclei does not indicate softness. The effect can be understood in terms of a simple model with parameters that are compatible with calculated quantities of the folded-Yukawa single-particle potential. To obtain further insight into the structure of these

asymmetric nuclear ground states, it is desirable to perform additional theoretical and experimental spectroscopic studies as suggested above.

References

1) F. Stephens, F. Asaro and I. Perlman, Phys. Rev. **96** (1954) 1568; **100** (1955) 1543
2) K. Alder, A. Bohr, T. Huus, B. Mottelson and A. Winther, Rev. Mod. Phys. **28** (1956) 432, and R.F. Christy, quoted therein
3) K. Lee and D.R. Inglis, Phys. Rev. **108** (1957) 774; **120** (1960) 1298
4) S. Suekane, Prog. Theor. Phys. **21** (1959) 74
5) I. Dutt and D. Mukherjee, Phys. Rev. **124** (1961) 888; Prog. Theor. Phys. **22** (1959) 814
6) S.A.E. Johansson, Nucl. Phys. **22** (1961) 529
7) M.L. Rustgi and S.N. Mukherjee, Phys. Rev. **131** (1963) 2615
8) H.J. Krappe and H.G. Wahsweiler, Nucl. Phys. **A104** (1967) 633
9) P. Vogel, Nucl. Phys. **A112** (1968) 583
10) J. Eichler and A. Faessler, Nucl. Phys. **A157** (1970) 166
11) L. Satpathy, H. Friedrich and A. Weiguny, J. de Phys. **32** (1971) C6–269
12) N. Onishi and R.K. Sheline, Nucl. Phys. **A165** (1971) 180
13) P. Möller, S.G. Nilsson and R.K. Sheline, Phys. Lett. **40B** (1972) 329
14) P. Möller, Nucl. Phys. **A192** (1972) 529
15) G. Leander and S.E. Larsson, Nucl. Phys. **A239** (1975) 93
16) C.G. Andersson, R. Bengtsson, T. Bengtsson, J. Krumlinde, G. Leander, K. Neergård, P. Olanders, J.A. Pinston, I. Ragnarsson, Z. Szymański and S. Åberg, Phys. Scripta **24** (1981) 266
17) J.P. Davidson, Rev. Mod. Phys. **37** (1965) 105
18) A. Arima and F. Iachello, Ann. of Phys. **99** (1976) 523
19) S.G. Rohoziński, J. of Phys. **G4** (1978) 1075
20) G. van den Berghe and H.E. de Meyer, Nucl. Phys. **A323** (1979) 302
21) K. Sage and J. Wood, private communication
22) V.G. Soloviev and P. Vogel, Phys. Lett. **6** (1963) 126
23) C.J. Veje, Mat. Fys. Medd. Dan. Vid. Selsk. **35** (1966) no. 1
24) L.A. Malov, V.G. Soloviev and P. Vogel, Phys. Lett. **22** (1966) 441
25) K. Neergård and P. Vogel, Nucl. Phys. **A145** (1970) 33; **A149** (1970) 209, 217
26) S.P. Ivanova, A.L. Komov, L.A. Malov and V.G. Soloviev, Bull. Acad. Sci. USSR (phys. ser.) **39** (1975) 130 [Izv. Akad. Nauk SSSR (ser. Fiz.) **39** (1975) 1286]
27) P. Möller and J.R. Nix, Nucl. Phys. **A361** (1981) 117
28) W. Kurcewicz, E. Ruchowska, N. Kaffrell, T. Björnstad and G. Nyman, Nucl. Phys. **A356** (1981) 15
29) R. Zimmermann, thesis, Munich, 1980
30) R.R. Chasman, Phys. Rev. Lett. **42** (1979) 630; Phys. Lett. **96B** (1980) 7
31) A. Gyurkovich, A. Sobiczewski, B. Nerlo-Pomorska and K. Pomorski, Phys. Lett. **105B** (1981) 95
32) P. Olanders, graduation thesis, Dept. of Math. Physics, Lund, 1977
33) M. Bolsterli, E.O. Fiset, J.R. Nix and J.L. Norton, Phys. Rev. **C5** (1972) 1050
34) P. Möller, S.G. Nilsson and J.R. Nix, Nucl. Phys. **A229** (1974) 292
35) A. Bohr and B.R. Mottelson, Nuclear structure, vol. 2 (Benjamin, New York, 1975)
36) H.J. Krappe, J.R. Nix and A.J. Sierk, Phys. Rev. **C20** (1979) 992
37) S.G. Nilsson, C.F. Tsang, A. Sobiczewski, Z. Szymański, S. Wycech, Ch. Gustafsson, I.L. Lamm, P. Möller and B. Nilsson, Nucl. Phys. **A131** (1969) 1
38) R.K. Sheline, Phys. Rev. **C21** (1980) 1660
39) J.F. Niello, H. Puchta, F. Riess and W. Trautmann, Annual Report (Jahresbericht), Beschleunigerlaboratorium der Universität und der Technischen Universität München (1980) p. 71;
J.F. Niello, private communication to R.K. Sheline, August, 1981
40) J.F.W. Jansen, Z. Sujkowski, D. Chmielewska and R.J. de Meijer, Proc. Int. Conf. on nuclei far from stability, Cargèse, France, 1976 (CERN 76-13) p. 415

41) L.K. Peker, J.H. Hamilton and J.O. Rasmussen, Phys. Rev. **C24** (1981) 1336
42) P. Möller and J.R. Nix, Nucl. Data Tables, **26** (1981) 165
43) E. Merzbacher, Quantum mechanics (Wiley, NY, 1961, 1970) ch. 5
44) G. Leander and R.K. Sheline, current work
45) H.J. Krappe and U. Wille, Nucl. Phys. **A124** (1969) 641
46) T. von Egidy, G. Barreau, H.G. Börner, W.F. Davidson, J. Larysz, D.D. Warner, P.H.M. van Assche, K. Nybø, T.F. Thorsteinsen, G. Løvhøiden, E.R. Flynn, J.A. Cizewski, R.K. Sheline, D. Decman, D.G. Burke, G. Sletten, N. Kaffrell, W. Kurcewicz and T. Björnstad, Nucl. Phys. **A365** (1981) 26
47) L.A. Kroger and C.W. Reich, Nucl. Phys. **A259** (1976) 29
48) I. Ahmad, A.M. Friedman, R.R. Chasman, R.R. Betts, J.E. Grindler and H.C. Griffin, Bull. Am. Phys. Soc. **26** (1981) 1118
49) I. Ragnarsson, S.G. Nilsson and R.K. Sheline, Phys. Reports **45** (1978) 1
50) I. Ragnarsson, Proc. Int. Symp. on future directions in studies of nuclei far from stability, Nashville, 1979 (North-Holland, Amsterdam, 1980) p. 367
51) T. Bengtsson, M.E. Faber, G. Leander, P. Möller, M. Ploszajczak, I. Ragnarsson and S. Åberg, Phys. Scripta **24** (1981) 200
52) S.M. Scott, W.D. Hamilton, D. Hungerford, D.D. Warner, G. Jung, K.D. Wünsch and B. Pfeiffer, J. of Phys. **G6** (1980) 1291
53) W.B. Walters, C. Chung, D.S. Brenner, R. Gill, M. Shmid, R. Chrien, H.-I. Liou, G. Gowdy, M. Stelts, Y.Y. Chu, F.K. Wohn, K. Sistemich, H. Yamamoto and R. Petry, Proc. Int. Conf. on nuclei far from stability, Helsingør, 1981 (CERN 81–09) p. 557